International Journal of Environmental Sciences ISSN: 2229-7359 Vol. 11 No. 18s, 2025 https://theaspd.com/index.php

Tailoring Structural And Electrochemical Behaviour Of Co Doped Mgfe₂O₄ Nanoparticles: A Co-Precipitation Approach

R.M.Regma Infant¹, S.R. Gibin^{2,3}, Joselin Beaula T^{4,6}, J.Samuel⁵

- ¹Research Scholar, Department of Physics and Research Centre, Malankara Catholic College, Mariagiri, Kaliakkavilai-629153, Tamil Nadu, India.
- ²Formerly Assistant Professor, Department of Physics and Research Centre, Malankara Catholic College, Mariagiri 629153, Tamil Nadu, India
- ³Associate Professor of Physics, Sree Sakthi Engineering College (Autonomous), Karamadai, Coimbatore-641104, Tamil Nadu, India
- ⁴Assistant Professor, Department of Physics and Research Centre, Malankara Catholic College, Mariagiri 629153, Tamil Nadu, India
- ⁵Associate Professor of Physics, Cape Institute of Technology Levengipuram-627114, Tamil Nadu, India.
- ⁶Manonmaniam Sundaranar University, Abishekapatti-627012, Tirunelveli, Tamil Nadu, India.

Abstract

Nano-sized Co-doped MgFe₂O₄ was effectively synthesized via a cost-effective co-precipitation method. Systematic characterization was carried out by using X-ray diffraction (XRD), transmission electron microscopy (TEM), scanning electron microscopy (SEM) coupled with energy-dispersive X-ray spectroscopy (EDX), X-ray photoelectron spectroscopy (XPS), and Fourier-transform infrared spectroscopy (FTIR). The XRD and FTIR results confirmed the evaluation of a spinel structure in the synthesized material. XPS investigation verified the presence of Co 2p, Fe 2p, Mg 2p, and O Is elements in the nanoparticles, indicating successful cobalt incorporation. Electrochemical impedance spectroscopy revealed that the capacitance behavior of the Co-doped MgFe₂O₄ electrodes improved with increasing temperature. Furthermore, cyclic voltammetry (CV) analysis demonstrated the highest specific capacitance at a scan rate of 2 mV/s. These findings suggest that the synthesized Co-doped MgFe₂O₄ nanoparticles exhibit promising electrochemical properties, suitable for supercapacitor applications.

Keywords: Nano-sized material, Co-precipitation technique, Spinel structure, Impedance, Supercapacitor.

1. INTRODUCTION

In recent years, nano-sized ferrites they have considerable attention owing to their remarkable magnetic, electrical, and thermal characteristics. Among them, magnesium ferrite, which crystallizes in a partially inverse spinel structure with a cubic spinel structure, stands out for its versatility [1]. Nanoscale magnesium ferrite exhibits unique characteristics that make it suitable for a variety of purposes, including high-density data storage, high-frequency electronic devices, and magnetic refrigeration systems [2]. Various synthetic techniques have been employed to produce nano-sized spinel ferrites, such as co-precipitation, sol-gel processing, microemulsion, hydrothermal synthesis, and reverse micelle methods [3-6].

Nanostructured magnetic materials have attracted growing their interest is due distinct properties compared to their bulk counterparts [7]. Specifically, ordered magnetic nanostructures like nanorods and nanowires have shown enhanced electrical and thermal behaviours, which are advantageous for advanced technological applications [8]. Although magnesium ferrite nanostructures have predominantly been synthesized in nanoparticle form, other morphologies such as nanorods or nanofibers remain relatively unexplored. Nano structuring, especially as a result of nanofibers, significantly increases the volume to surface ratio, which can enhance their performance in applications such as nanocomposites, catalysis, sensing, nanoelectronics, and photonic devices [9,10].

Enhancing the electrical and physicochemical characteristics essential for energy storage devices like supercapacitors and batteries has been made possible in large part by nanotechnology. [11]. The development of new electronic systems demands advanced materials with multifunctional capabilities [12]. Supercapacitors, in particular, are emerging as efficient energy storage devices due to their ability to deliver high power, integrate well with renewable energy sources, and offer long operational lifespans [13,14]. They present several advantages over traditional energy storage systems like batteries and dielectric capacitors, including higher power density and greater cycling stability.

International Journal of Environmental Sciences

ISSN: 2229-7359 Vol. 11 No. 18s, 2025

https://theaspd.com/index.php

Among the various synthesis methods, co-precipitation has gained prominence over the last two decades for its ability to produce oxide materials with controlled composition and uniform particle size. In the present study, we report the synthesis of cobalt-substituted magnesium ferrite using an optimized co-precipitation technique. The structural properties of the samples were initially investigated using X-ray diffraction (XRD). Thermal analysis through thermogravimetric and differential thermal (TG/DTA) methods guided the selection of annealing temperature, with samples treated at 700 °C undergoing further detailed characterization. These analyses included scanning electron microscopy (SEM), high resolution transmission electron microscopy (HR-TEM), cyclic voltammetry (CV), Brunauer Emmett–Teller (BET) surface area analysis, Fourier-transform infrared spectroscopy (FTIR), and X-ray photoelectron spectroscopy (XPS). These methods, when combined, offered a comprehensive understanding of the structural, morphological, electrochemical, surface, and chemical properties of the Co-doped magnesium ferrite nanoparticles produced.

2.Experimental

2.1Synthesis of Co doped MgFe₂O₄ nanoparticles

The Co-doped MgFe₂O₄ nanoparticles were synthesized using a modified co-precipitation method, with MgFe₂O₄ serving as the base material. All reagents were procured from Merck Chemicals and used without further purification. Initially, magnesium nitrate [Mg(NO₃)₂·4H₂O], iron nitrate [Fe(NO₃)₃·9H₂O], and citric acid (C₆H₈O₇) were each dissolved in 20 mL of deionized water. The resulting solutions were subsequently combined and stirred, while sodium hydroxide (NaOH) was gradually added dropwise to commence precipitation. The mixture was kept under continuous stirring at 80 °C for 30 minutes.

Subsequently, a 0.01 M solution of cobalt nitrate was introduced into the reaction mixture, followed by stirring at 80 °C for an additional 3 hours. Citric acid acted as a chelating agent throughout the process, promoting the formation of stable complexes and aiding the uniform precipitation of metal ions. This process resulted in the creation of brown-colored precipitates. These precipitates were thoroughly washed with deionized water and acetone to eliminate impurities, followed by drying at 80 °C to yield a dark brown powder. Ultimately, the dried material was calcined at 700 °C for a duration of 3 hours in a muffle furnace to attain the required crystalline phase.

2.2Characterization techniques

X-ray diffraction (XRD) analysis was performed to examine the crystalline phase of Co-doped MgFe₂O₄ nanoparticles. Measurements were carried out utilizing a BRUKER D8 Advance Davinci diffractometer (USA) that is equipped with CuK α radiation (λ = 1.54060 Å), functioning at 40 kV and 30 mA. For the analysis of surface morphology, a scanning electron microscope (SEM) (CARL ZEISS EVO 18) was employed after the samples were sputter-coated with a conductive layer. High-resolution transmission electron microscopy (HR-TEM), along with energy dispersive X-ray spectroscopy (EDX), was utilized to assess particle size, morphology, and elemental composition. The HR-TEM analysis was conducted using an FEI TECNAI G2 - 20 TWIN microscope operating at an accelerating voltage of 200 kV. The elemental composition was further validated using a Bruker EDX system that is equipped with an LN_2 -free detector. Furthermore, selected area electron diffraction (SAED) patterns were acquired by positioning the sample on a carbon-coated copper grid. X-ray photoelectron spectroscopy (XPS) was employed to ascertain the surface chemical composition and oxidation states of elements, utilizing an ULVAC-PHI INC PHI5000 (probe version 111). The Brunauer-Emmett-Teller (BET) surface area and pore size distribution were evaluated using the Quantachrome Autosorb IQ series instrument. Fourier-transform infrared spectroscopy (FTIR) was conducted with a PerkinElmer Spectrum Two spectrometer to identify functional groups and validate the spinel structure. The thermal stability and decomposition characteristics of the nanoparticles were examined through thermogravimetric and differential thermal analysis (TG/DTA), executed on a NETZSCH STA 449 F3 JUPITER system. The electrochemical performance was assessed through cyclic voltammetry (CV) using a Versa STAT MC electrochemical workstation to evaluate the capacitance behaviour of the synthesized material.

3. RESULTS AND DISCUSSION

3.1 XRD analysis

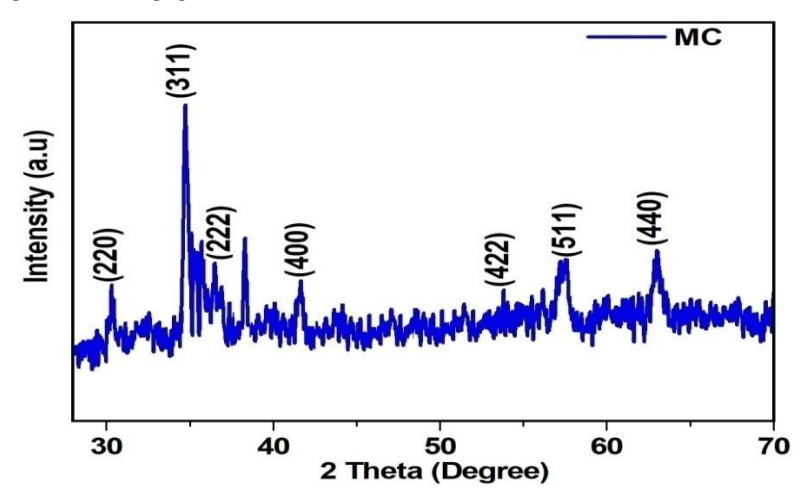


Fig. 1 X-ray diffraction patterns of Co doped MgFe₂O₄ nanoparticles

Figure 1 illustrates the X-ray diffraction (XRD) pattern of Co-doped MgFe₂O₄ nanoparticles that were synthesized through the co-precipitation method and subsequently annealed at 700 °C. The diffraction peaks observed correspond to the (220), (311), (400), (422), (511), and (440) planes, which indicate a face-cantered cubic spinel structure with the space group Fd-3m, thereby confirming the successful formation of the spinel phase. The average crystallite size (D) was estimated using the (311) diffraction peak and was calculated by employing Scherrer's equation [15].

$$D = \frac{0.94 \,\lambda}{\beta_D \cos \theta} \tag{1}$$

Where βD represents the full width at half maximum (FWHM) of the diffracting peak, λ denotes the wavelength of X-ray (0.1541 nm), and θ signifies the Bragg's diffraction angle. The crystallite sizes of the sintered ferrites were measured to be within the range of 47 nm.

3.2 TEM analysis

The TEM image of the Co-doped MgFe₂O₄ nanoparticles (Fig. 2(a)) reveals that the particles are well-dispersed, exhibiting a rod-like morphology with random orientation. The average length and diameter of the nanoparticles are observed to be below 50 nm and 10 nm, respectively. The high-resolution transmission electron microscopy (HRTEM) image presented in Fig. 2(b) reveals clear lattice fringes, thereby affirming the crystalline characteristics of the material. The measured lattice spacing corresponding to the (311) plane is approximately 0.25 nm, which aligns closely with the d-spacing value obtained from XRD analysis. The selected area electron diffraction (SAED) pattern (Fig. 2(c)) displays well-defined concentric rings characteristic of a cubic spinel structure, with no evidence of secondary phases. The diffraction rings match well with standard reference data (JCPDS card no. 36-1451) for MgFe₂O₄, further verifying phase purity and crystallinity.

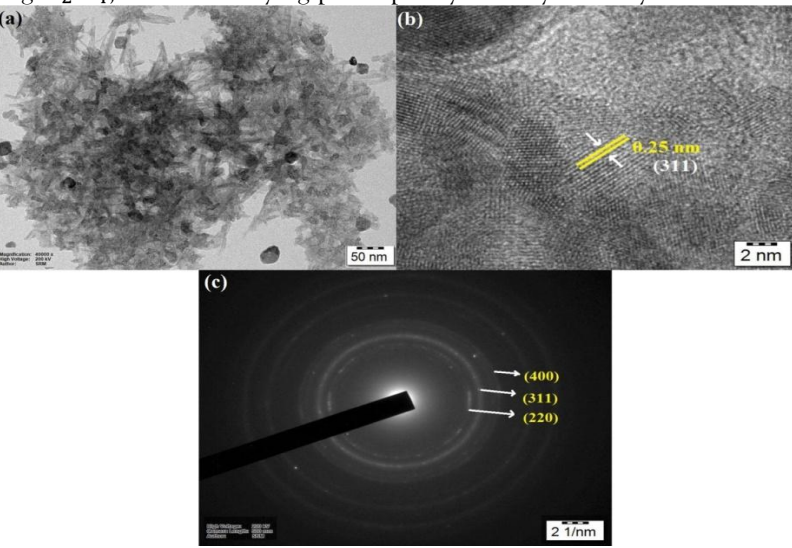


Fig. 2 (a) TEM micrographs (b) HRTEM image and (c) Selected area electron diffraction (SAED) pattern of Co doped $MgFe_2O_4$ nanoparticles 3.3 SEM and EDX analyses

https://theaspd.com/index.php

Figure 3 illustrates the elemental mapping of Co-doped MgFe₂O₄ nanoparticles, confirming the uniform spatial distribution of magnesium (Mg), iron (Fe), cobalt (Co), and oxygen (O) throughout the sample. To further verify this homogeneous distribution, spot EDS (energy-dispersive X-ray spectroscopy) analysis was performed, and the corresponding results are presented in Figures 3(b) and 3(c). The EDX spectrum clearly displays distinct peaks corresponding to Mg, Fe, Co, and O, validating the elemental composition of the synthesized nanoparticles. Strong signals for Mg, Fe, and O are observed, with Co also being distinctly detected, indicating successful doping. Additionally, minor peaks may be attributed to trace impurities, likely originating from the sample holder or surrounding environment during analysis.

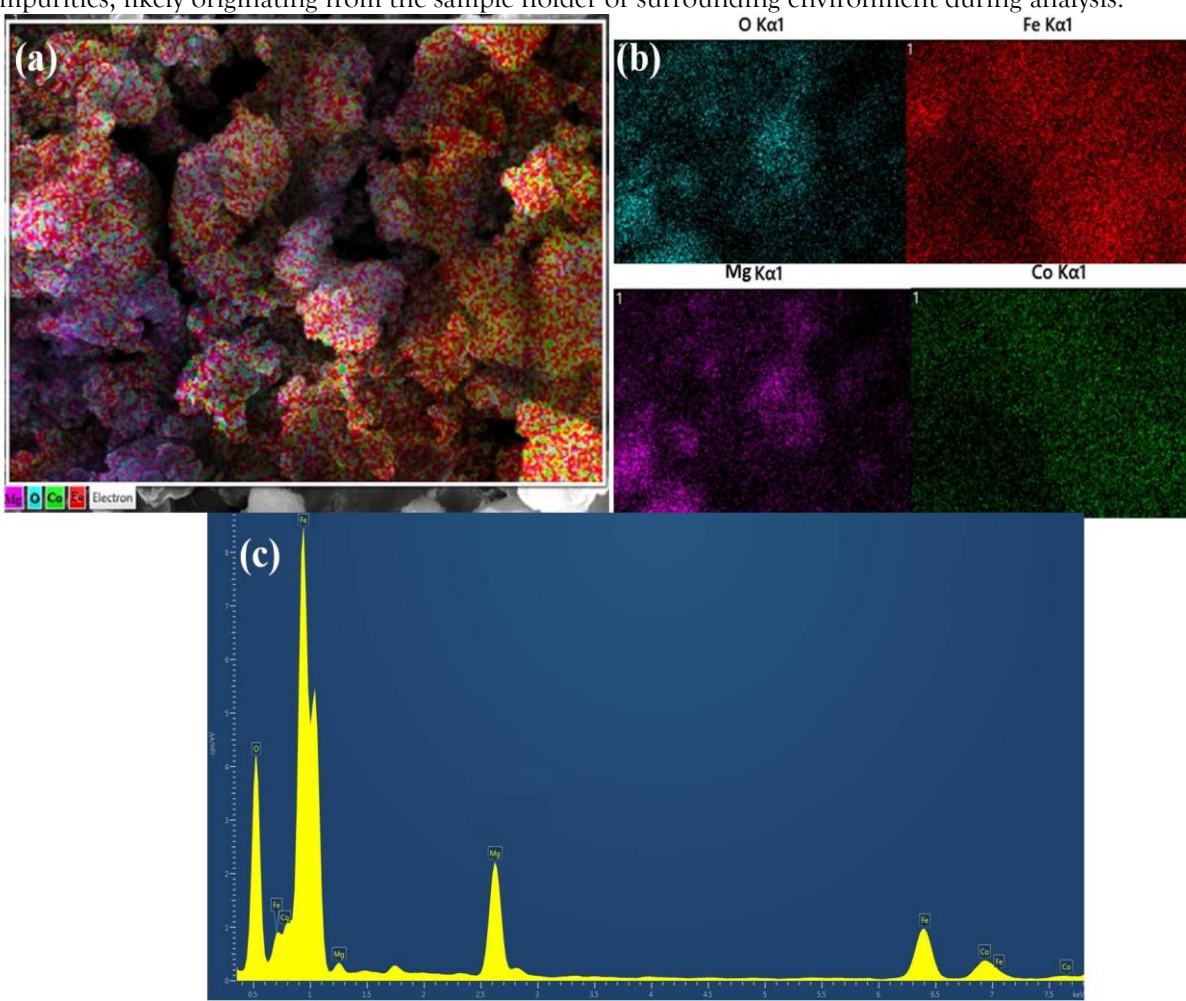


Fig. 3 Scanning electron microscope (SEM) images and energy-dispersive x-ray spectrometer (EDX) elemental maps of the Co doped MgFe₂O₄ nanoparticles

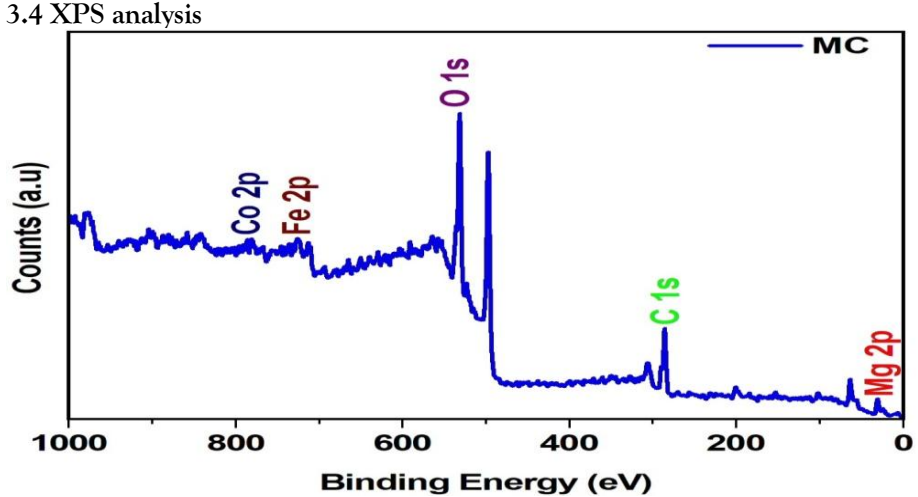


Fig. 4 (a) X-ray photoemission survey spectrum of Co doped MgFe₂O₄ nanoparticles

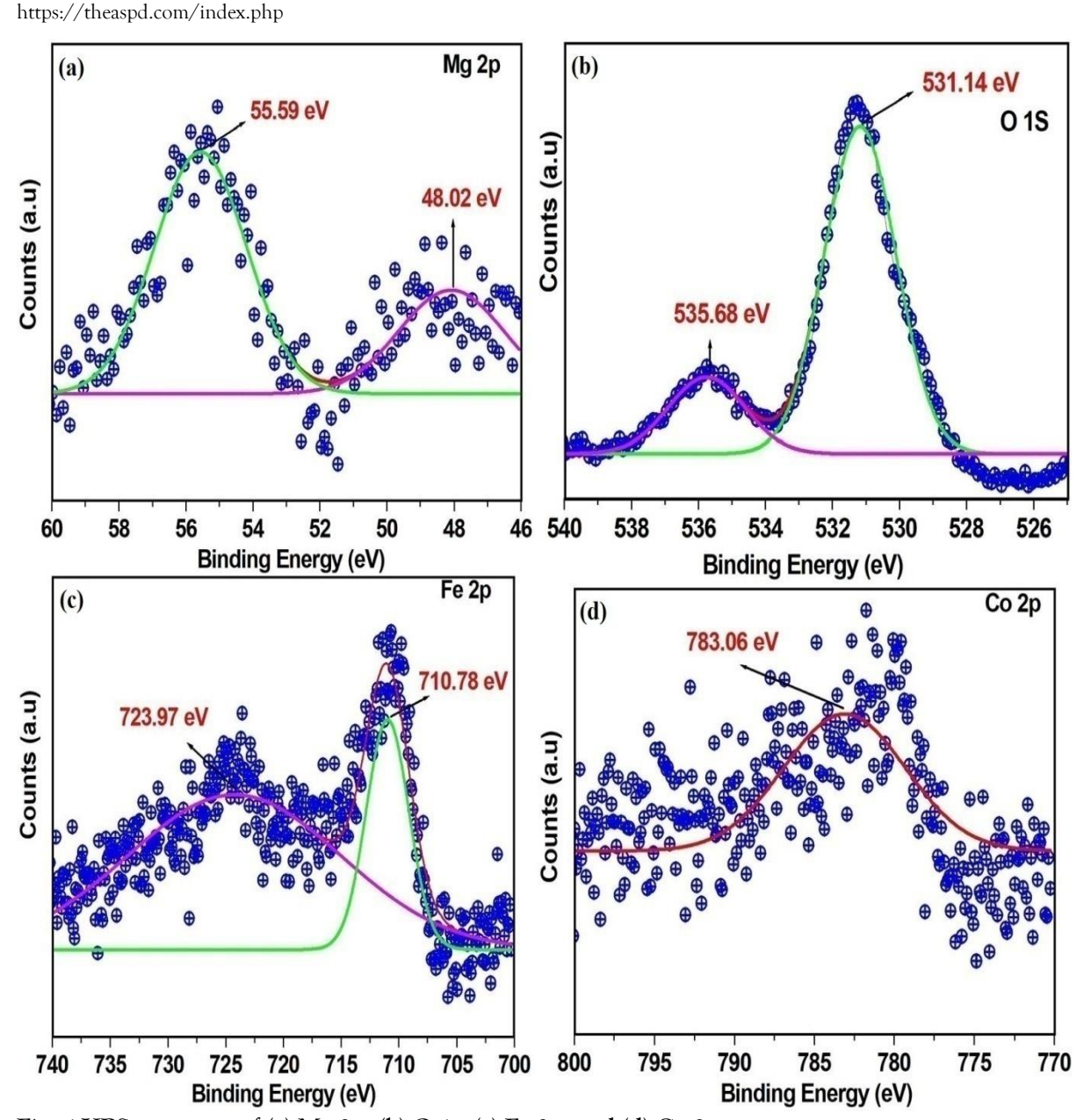


Fig. 5 XPS spectrum of (a) Mg 2p, (b) O 1s, (c) Fe 2p, and (d) Co 2p

X-ray Photoelectron Spectroscopy (XPS) was utilized to determine the surface elemental composition, oxidation states, and binding energies of the Co-doped MgFe₂O₄ nanoparticles. The wide-scan XPS spectrum (Fig. 4) verifies the presence of Co, Fe, Mg, O, and a minor signal from carbon (C). The C 1s peak appearing at 284.31 eV is generally attributed to adventitious carbon contamination resulting from exposure to the atmosphere. To obtain a more detailed understanding of the chemical states of the individual elements, high-resolution XPS spectra were recorded for Mg 2p, O 1s, Fe 2p, and Co 2p, as illustrated in Figures 5(a–d). The Mg 2p spectrum (Fig. 5a) displays two peaks at binding energies of 55.59 eV and 48.02 eV, corresponding to Mg 2p₃/₂ and Mg 2p₁/₂, respectively, indicating the presence of Mg²⁺ ions. The O 1s spectrum (Fig. 5b) is deconvoluted into two separate peaks: one at 530.20 eV, which is attributed to lattice oxygen in the spinel structure, and another at 531.21 eV, likely linked to surface hydroxyl groups or adsorbed oxygen. The Fe 2p spectrum (Fig. 5c) displays two prominent peaks at 710.78 eV and 723.97 eV, corresponding to Fe 2p₃/₂ and Fe 2p₁/₂, respectively, confirming the presence of iron in the +3 oxidation state within the ferrite matrix. In the Co 2p region (Fig. 5d), peaks associated with Co²⁺ are observed, suggesting that cobalt ions have successfully substituted into the MgFe₂O₄ lattice without the formation of secondary phases or metallic Co clusters.

Overall, the XPS results confirm the successful incorporation of Co^{2^+} into the spinel structure, with all elements present in their expected oxidation states, supporting the formation of a phase-pure Co-doped MgFe₂O₄ material [18].

https://theaspd.com/index.php

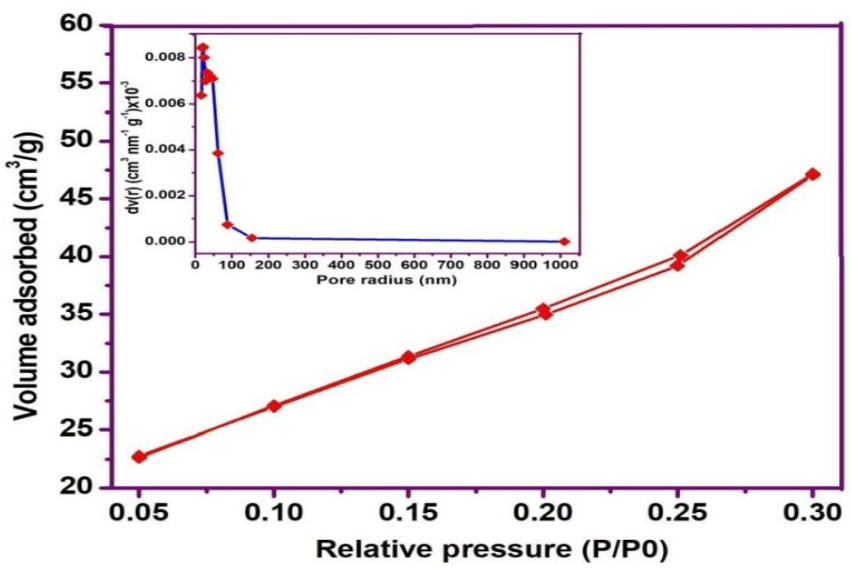


Fig. 6 N₂ adsorption-desorption isotherm of nanoparticles.

Figure 6 displays the nitrogen (N_2) adsorption-desorption isotherm for Co-doped MgFe $_2$ O $_4$ nanoparticles, illustrating the material's surface adsorption characteristics. The isotherm corresponds to a type IV profile with an H2 hysteresis loop, as classified by the IUPAC system, which is indicative of mesoporous materials. The observed hysteresis suggests the presence of disordered mesopores within the Co-doped MgFe $_2$ O $_4$ structure.

Brunauer-Emmett-Teller (BET) analysis reveals a specific surface area of 45.87 m² g⁻¹, which is notably higher than values reported in earlier studies for similar materials [19, 20]. The pore size distribution curve, shown in the inset of Fig. 6, highlights a predominant pore size of approximately 3.13 nm. Additionally, the mesoporous range is observed to extend from 21 nm to 93 nm, confirming a heterogeneous porosity distribution.

The high surface area and well-developed mesoporous structure of the Co-doped MgFe₂O₄ nanoparticles provide abundant active sites, which are advantageous for enhancing electrochemical performance, particularly in applications such as supercapacitors.

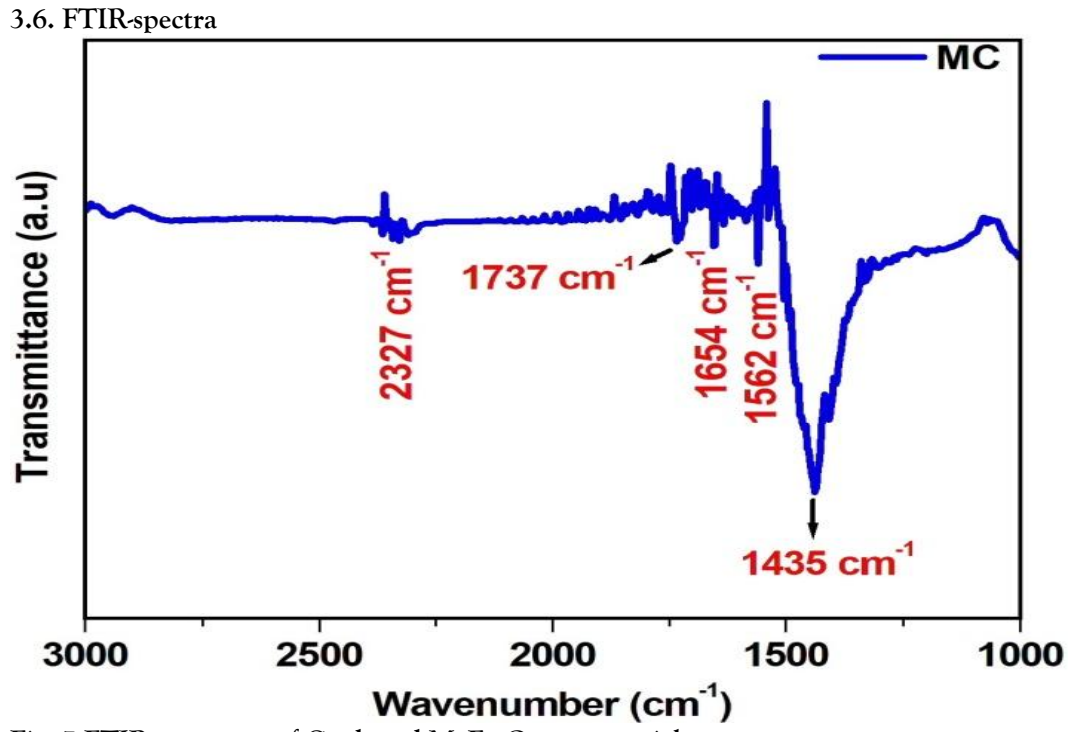


Fig. 7 FTIR spectrum of Co doped MgFe₂O₄ nanoparticles

The FTIR spectrum of Co-doped $MgFe_2O_4$ nanoparticles is presented in Figure 7. Fourier Transform Infrared (FTIR) spectroscopy serves as an effective tool to confirm the formation of the spinel ferrite structure. The absorption band observed at higher wavenumbers corresponds to the stretching vibrations

of metal-oxygen bonds located in the tetrahedral (A) sites of the spinel lattice. In contrast, the lower-frequency band is attributed to the vibrations of metal-oxygen bonds in the octahedral (B) sites [21]. These distinct vibrational features further affirm the successful formation of the spinel structure in the synthesized Co-doped MgFe₂O₄ nanoparticles. The FTIR results thus provide strong evidence supporting the presence of a well-defined spinel phase Furthermore, absorption bands identified around 3000 cm⁻¹ and 1000 cm⁻¹ are linked to the stretching and bending vibrations of H-O-H bonds, suggesting the existence of physically adsorbed or residual water within the sample. Peaks observed around 1400 cm⁻¹ and 1654 cm⁻¹ are ascribed to the bending vibrations of water molecules, further validating the moisture content present in the nanoparticles [22]. The band located at 1562 cm⁻¹ denotes the C-H bending modes [23]. A prominent absorption peak was detected at 1737 cm⁻¹, affirming the presence of O-H groups in the sample [24]. Additionally, the peak at 2327 cm⁻¹ indicates the O-H stretching vibration of the absorbed water molecule [25].

3.7 Thermogravimetric and differential thermal analysis (TG/DTA)

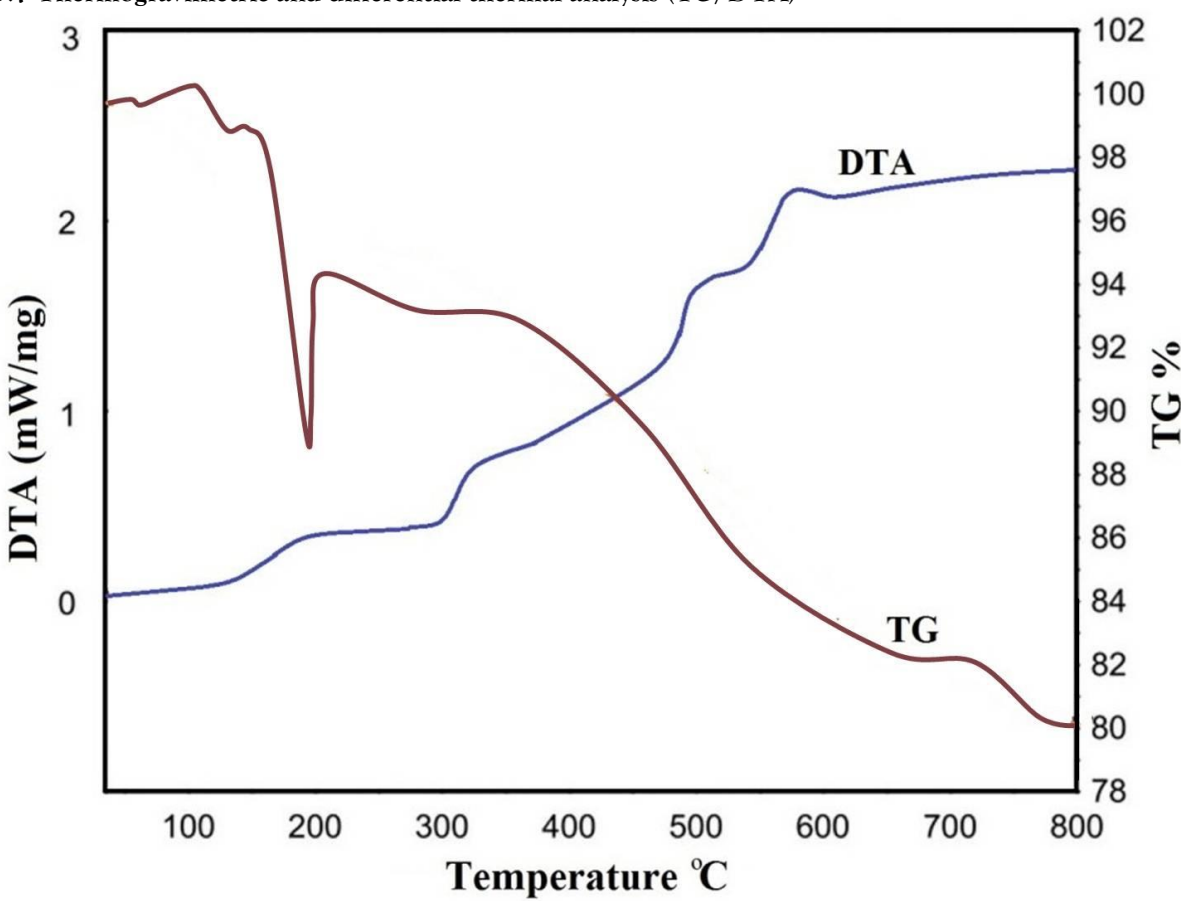


Fig. 8 TG/DT analysis curve of Co doped MgFe₂O₄ nanoparticles.

The thermal stability and decomposition characteristics of the Co-doped MgFe₂O₄ nanoparticles were assessed through simultaneous Thermogravimetric Analysis (TGA) and Differential Thermal Analysis (DTA) over a temperature range of 35 °C to 850 °C, as depicted in Figure 8.

The TGA curve indicates an initial weight reduction of about 4% occurring between 40 °C and 215 °C, which is mainly due to the evaporation of physically adsorbed water molecules. A subsequent weight loss of approximately 12% is noted between 215 °C and 650 °C, probably resulting from the decomposition of organic residues or citric acid utilized during the synthesis [26].

A third weight loss of nearly 2% in the range of 500 °C to 680 °C may correspond to structural rearrangements or phase transitions within the Co-doped MgFe₂O₄ lattice. A final and more significant weight loss of about 33% occurs between 680 °C and 780 °C, indicating the formation and crystallization of the cobalt-doped magnesium ferrite phase.

The corresponding DTA curve shows an endothermic peak near 85 °C, which is associated with the dehydration process. Additionally, a prominent exothermic peak at approximately 240 °C is observed, suggesting the decomposition of residual nitrate precursors in the sample. [27].

3.8 Cyclic Voltammetry

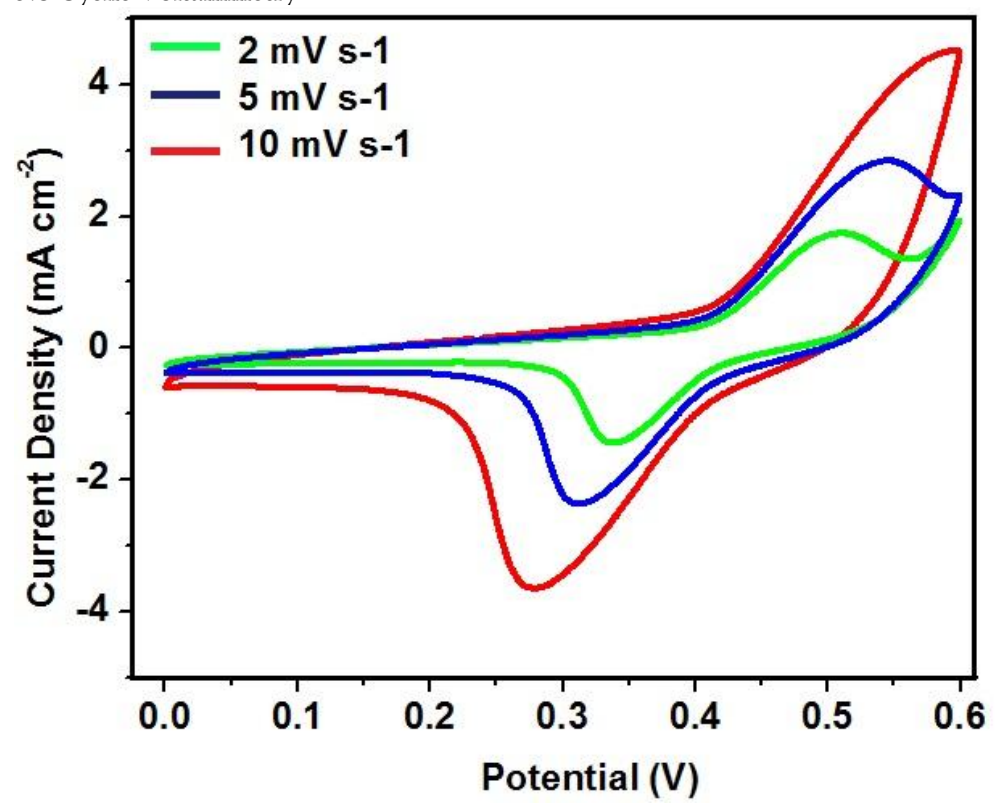


Fig. 9 CV pattern of Co doped MgFe₂O₄ nanoparticles.

The electrochemical measurements were performed using a standard three-electrode setup, which included a sample functioning as the working electrode, an Ag/AgCl reference electrode, and a high platinum wire serving as the counter electrode [28]. In this study, 0.2 M tetra butyl ammonium perchlorate was utilized as the electrolyte. The capacitive characteristics of a Co-doped MgFe₂O₄ electrode were investigated using cyclic voltammetry (CV) as an electrochemical method. Figure 9 illustrates the current density in relation to the applied potential when exposed to visible light irradiation. The CV measurements were conducted at different scan rates of 2, 5, and 10 mVs⁻¹, with the findings presented in Fig. 9. At lower scan rates, the CV curves display an ideal rectangular shape, indicative of well-defined capacitive behaviour [29]. The cyclic voltammetry (CV) patterns of the Co-doped MgFe₂O₄ sample, which was subjected to calcination at 700 °C, demonstrate a pseudo-capacitive characteristic, as shown by the alterations in the CV curves with an increasing scan rate. This suggests the existence of pseudo-capacitive processes within the system, reflecting a dynamic capacitive response that is affected by the scan rate. The specific capacitance (Cs) value of the synthesized Co-doped MgFe₂O₄ electrode was calculated using the following equation [30].

$$Cs = \frac{Q}{\Delta v.m} \tag{2}$$

Here, Q stands for the anodic and cathodic charges that are measured during each cyclic voltammetry (CV) scan, and C_s indicates the electrode material's specific capacitance. The constant scan rate (mV s⁻¹) used for the measurements is indicated by Δv , whereas the variable m represents the mass of the active electrode material (in mg). Every CV analysis was performed within the 0.0–0.6 V potential window.

The nearly perfect rectangular shape of the CV profile of virgin Co-doped MgFeO₄ is indicative of capacitive behaviour and is linked to faradaic redox reactions that take place at the active electrode surface. The electrode material's pseudocapacitive properties are further supported by the existence of two separate redox peaks [31]. The oxidation and reduction peak current densities increase proportionately when the scan rate is increased from low to high values, as seen in Fig. 9, and peak positions slightly move as well. The quick and reversible redox reactions taking place on the electrode surface are the cause of this change. Notably, the CV curves show good electrochemical reversibility even at a rather high scan rate of 10 mV s^{-1} , maintaining their shape without noticeable distortion.

One significant finding was that the specific capacitance was highest at the lowest scan rate. This suggests that electrolyte ions had enough time to diffuse into the porous electrode structure's inner and outer surfaces at slower scan rates. The effective use of the electrode's active sites is decreased with higher scan

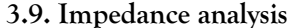
International Journal of Environmental Sciences ISSN: 2229-7359

Vol. 11 No. 18s, 2025

https://theaspd.com/index.php

rates, however, because ion transport is primarily restricted to the outer surface. Improved charge storage is made possible by the co-doping in MgFeO₄, which seems to increase the active surface area.

Electric double-layer capacitance and faradaic redox contributions are thus both involved in the charge storage mechanism, with the latter being more prominent because of the pseudocapacitive behaviour brought on by Co inclusion. The electrode at 2 mV s⁻¹ shows the highest Capacitive double layer among the measured scan rates, demonstrating successful electron-hole separation and charge carrier transport at the electrode-electrolyte interface. At scan speeds of 2, 5, and 10 mV s⁻¹, the observed specific capacitance values are 323 F g⁻¹, 207 F g⁻¹, and 161 F g⁻¹, respectively. This pattern shows that greater capacitance values can be obtained at reduced scan rates, which is very useful for high-performance supercapacitor applications [32].



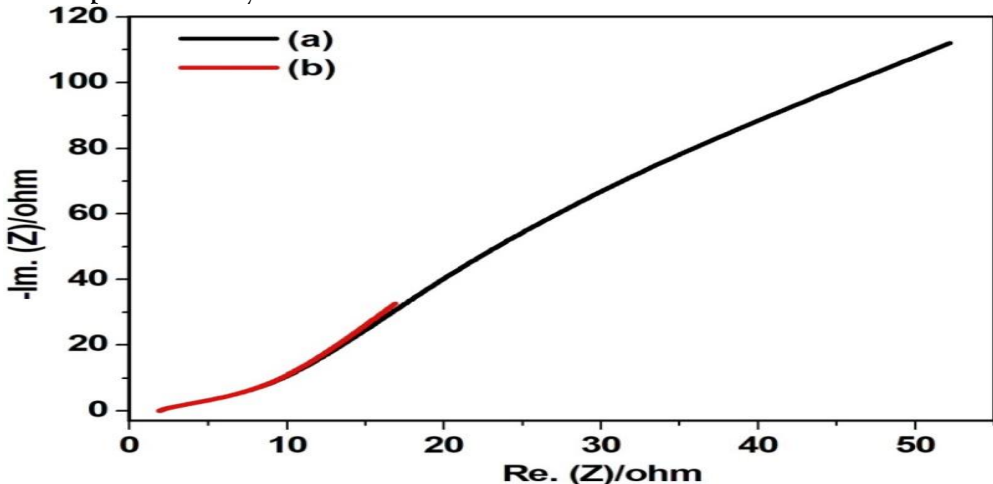


Fig. 10 Variation between Re. (Z) and -Im. (Z) of Co doped MgFe₂O₄ nanoparticles at different temperatures (a) 100 °C and (b) 150 °C

The electrochemical impedance analysis was conducted on the ion transfer pathways and the conductivity of the Co doped MgFe₂O₄ electrode materials. Figure 10 illustrates the Nyquist plots for Co doped MgFe₂O₄ electrodes, which depict the real and imaginary components of the impedance spectra. Additionally, an analysis of the real and imaginary impedance provides insight into the presence of grains and grain boundaries. Consequently, the conduction may be categorized as long range or short ranged, that is, non-localized or localized charge transfer [33]. Shape of the Nyquist plots (Fig. 10) gives an idea about various conduction mechanisms and used to investigate relaxation behaviour of prepared samples. In a Nyquist plot, the existence of multiple semicircles indicates the presence of both grains and grain boundaries. The semicircle at low frequencies is attributed to the grains, while the semicircle at high frequencies is associated with the grain boundaries. Additionally, it is evident that the intercept point on the real axis shifts from the origin as the temperature rises, which implies a reduction in the resistive properties of the material [34]. This analysis provides insights into the bulk resistance (Rb) and the grain boundary resistance (Rgb) of the materials. This observation can be supported by the understanding that the influence of grains surpasses that of the grain boundaries in cobalt-doped magnesium ferrites [35, 36]. The impedance measurements indicate that Co-doped MgFe₂O₄ nanoparticles exhibit high conductivity, thereby minimizing the diffusion distance between the electrolyte and the electrode material.

4. CONCLUSION

In this research, Co-doped $MgFe_2O_4$ nanoparticles were effectively synthesized through the coprecipitation method, followed by annealing at $700\,^{\circ}$ C. X-ray diffraction analysis validated the development of a single-phase spinel structure exhibiting good crystallinity, with an estimated average crystallite size of around 47 nm. TEM and HRTEM images displayed a rod-like morphology with nanoscale dimensions and clearly defined lattice fringes, while SAED patterns confirmed the absence of any secondary phases. SEM-EDX mapping confirmed a uniform distribution of the constituent elements, further substantiating the successful incorporation of Co into the $MgFe_2O_4$ matrix.

XPS analysis confirmed the oxidation states of Mg²⁺, Fe³⁺, and Co²⁺ within the spinel framework, providing strong evidence for phase purity and chemical integrity. BET measurements revealed a high specific surface area of 45.87 m² g⁻¹ and mesoporous characteristics, which are beneficial for

International Journal of Environmental Sciences

ISSN: 2229-7359 Vol. 11 No. 18s, 2025

https://theaspd.com/index.php

electrochemical performance. FTIR spectra displayed characteristic metal-oxygen vibrations, further confirming the spinel structure, along with the presence of surface-adsorbed water and hydroxyl groups. Thermogravimetric and DTA analysis demonstrated the thermal stability and phase formation behaviour of the nanoparticles, with major weight loss steps corresponding to water evaporation and organic decomposition, followed by crystallization. Electrochemical impedance spectroscopy revealed improved ion transport with increasing temperature and highlighted both grain and grain boundary contributions to conductivity. Notably, the material exhibited high conductivity, suggesting reduced charge transfer resistance and efficient electron/ion transport pathways.

Finally, cyclic voltammetry studies indicated a pseudocapacitive behaviour with high specific capacitance values, particularly at lower scan rates (up to $323 \, \mathrm{Fg^{-1}}$ at $2 \, \mathrm{mV \, s^{-1}}$), making Co-doped MgFe₂O₄ a promising electrode material for supercapacitor applications.

REFERENCE

- 1. C. Choodamani, B. Rudraswamy and G. T. Chandrappa, Structural, electrical, and magnetic properties of Zn substituted magnesium ferrite, Ceram. Inter., 42 (2016)10565-10571.
- 2. S. Thankachan, S. Xavier, B. Jacob, and E. M. Mohammed, A comparative study of structural, electrical and magnetic properties of magnesium ferrite nanoparticles synthesised by sol-gel and co-precipitation techniques, J. Experimental Nanoscience, 8 (2013) 347–357.
- 3. E. Veena Gopalan, I.A. Al-Omari, K.A. Malini, P.A. Joy, D. Sakthi Kumar, Y. Yoshida, and M.R. Anantharaman, Impact of zinc substitution on the structural and magnetic properties of chemically derived nanosized manganese zinc mixed ferrites, J. Magn. Magn. Mater. 321 (2009) 1092–1099.
- 4. E. Veena Gopalan, K.A. Malini, S. Saravanan, D. Sakthi Kumar, Y. Yoshida, and M.R. Anantharaman, Evidence for polaron conduction in nanostructured manganese ferrite, J. Phys. D: Appl. Phys. 41 (2008) 185005-185016.
- 5. M. Srivastava, S. Chaubey, and A.K. Ojha, Investigation on size dependent structural and magnetic behavior of nickel ferrite nanoparticles prepared by sol-gel and hydrothermal methods, Mater. Chem. Phys. 118(1) (2009) 174–180.
- 6. Y. L. Liu, Z. M. Liu, Y. Yang, H. F. Yang, G. L. Shen, and R. Q. Yu, Simple synthesis of MgFe2O4 nanoparticles as gas sensing materials, Sens. Actuators B, 107 (2005) 600–604.
- 7. Z. Lai, G. Xu, Y. Zheng, Microwave assisted low temperature synthesis of MnZn ferrite nanoparticles, Nanoscale Res. Lett., 40 (2007).
- 8. Z. H. Hua, R. S. Chen, C. L. Li, S. G. Yang, M. Lu, X. B. Gu and Y. W. Du, CoFe₂O₄ nanowire arrays prepared by template-electrodeposition method and further oxidization, J. Alloys Compd. 427, 199 (2007).
- 9. S. Maensir, M. Sangmanee and A. Wiengmoon, Magnesium Ferrite (MgFe2O4) Nanostructures Fabricated by Electrospinning, Nanoscale Res Lett (2009) 4:221–228.
- 10. [6] U.S. Sharma, R.N. Sharma, R. Shah, Physical and magnetic properties of manganese ferrite nanoparticles, Int. J. Eng. Res. Afr., 4 (8) (2014) 14-17.
- 11. C. Sambathkumar, N. Nallamuthu, M. K. Kumar, S. Sudhahar and P. Devendran, Electrochemical exploration of cobalt sulfide nanoparticles synthesis using cobalt diethyldithiocarbamate as single source precursor for hybrid supercapacitor device, J. Alloys Compd., 920 (2022), 165839-165848.
- 12. A. Raza, K. Sayeed, A. Naaz, M. Muaz, S. N. Islam, S. Rahaman, F. Sama, K. Pandey and A. Ahmad, Green Synthesis of ZnO Nanoparticles and Ag-Doped ZnO Nanocomposite Utilizing Sansevieria trifasciata for HighPerformance Asymmetric Supercapacitors, ACS Omega, 9 (2024) 32444—32454.
- 13. K. Seevakan, A. Manikandan, P. Devendran, Y. Slimani, A. Baykal and T. Alagesan, Structural, magnetic and electrochemical characterizations of Bi2Mo2O9 nanoparticle for supercapacitor application, J. Magn. Magn. Magn. Mater. 486 (2019), 165254.
- 14. M. Murugesan, N. Nallamuthu, R. Ranjithkumar, M. Krishnakumar, P. Devendran and K. Ramesh, Synthesis and electrochemical investigation of hetero bimetallic complexes CoMn2O4 micro rods for novel supercapacitor electrode, Electron. Mater. Lett. 19 (1) (2023) 108–118.
- 15. B.D. Cullity, Elements of X-ray Diffraction, Addison-Wesley, London, 1959.
- 16. S. S. Guzman, B. R. Jayan, E. d. Rosa, A. T. Castro, V. G. Gonzalez and M. J. Yacaman, Synthesis of assembled ZnO structures by precipitation method in aqueous media, Mater. Chem. Phys., 115 (2009) 172-178.
- 17. M. Silva, V. Murzin, L. Zhang, J. Baltrus and J. Baltrusaitis, Transition Metal Doped MgO Nanoparticles for Nutrient Recycling: An Alternate Mg Source for Struvite Synthesis from Wastewater, Environmental Science: Nano, 7(2020)3482–3496. 18. Y. Zong, Y.Sun,S. Meng and X. Zheng, Doping effect and oxygen defects boost room temperature ferromagnetism of Codoped ZnO nanoparticles: Experimental and theoretical studies, RSC Adv., 9 (2019) 23012-23025.
- 19. A. Monunith, A. Rajan and N. K. Sahu, Comparative study of enzymatic and non-enzymatic detection of glucose using manganese ferrite nanoparticles, Mater. Res. Express 7 (9) (2020).
- 20. C. O. Ania, A. Gomis-Berenguer, J. Dentzer and C. Vix-Guterl, Nanoconfinement of glucose oxidase on mesoporous carbon electrodes with tunable pore sizes, J. Electroanal. Chem. 808 (2018) 372–379.
- 21. R. D. Waldron, Infrared spectroscopy of ferrites, Phy. Rev. 99 (1955), pp. 1727-1735.
- 22. L. A. Kafshgari, M. Ghorbani and A. Azizi, Synthesis and characterization of manganese ferrite nanostructure by coprecipitation, sol-gel, and hydrothermal methods, Particulate Sci. Technol. 37 (7) (2018) 904–910.
- 23. R. Sundari, T. I. Hua, M. Aziz and D. Nizar, The characterization study of ferrites (magnesium and manganese) using sol gel method, The Malaysian J. Analytical Sciences 18 (3) (2014) 485–490.
- 24. M. M. N. Ansari, S. Khan and N. Ahmad, Effect of R3+ (R= Pr, Nd, Eu and Gd) substitution on the structural, electrical, magnetic and optical properties of Mn-ferrite nanoparticles, J. Magn. Magn Mater. 465 (2018) 81–87.

International Journal of Environmental Sciences

ISSN: 2229-7359 Vol. 11 No. 18s, 2025

https://theaspd.com/index.php

- 25. A. M. Jacintha, V. Umapathy, P. Neeraja and S. R. J. Rajkumar, Synthesis and comparative studies of MnFe2O4 nanoparticles with different natural polymers by sol-gel method: structural, morphological, optical, magnetic, catalytic and biological activities, J. Nanostruct. Chem., 7 (2017) 375–387.
- 26. D. Abisha, S. R. Gibin, V. K. PremKumar and A. Mariappan, Improved supercapacitor application of manganese ferrite nanoparticles via co-precipitation technique, Heliyon, 9 (2023) 21120-21131.
- 27. P. Sivagurunathan and S. R. Gibin, Preparation and characterization of nanosized cobalt ferrite particles by co-precipitation method with citrate as chelating agent, J. Mater. Sci. Mater. Electron. 27 (2016) 8891–8898.
- 28. S. R. Gibin, P. Sivagurunathan, Synthesis and characterization of nickel cobalt ferrite (Ni1 xCox Fe2O4) nano particles by co-precipitation method with citrate as chelating agent, J. Mater. Sci. Mater. Electron. 28 (2017) 1985–1996.
- 29. K. Sathishkumar, N. Shanmugam, N. Kannadasan, S. Cholan and G. Viruthagiri, Opto, magnetic and electrochemical characterization of Ni1–xCoxO nanocrystals, J. Mater. Sci. Mater. Electron. 26 (2015) 1881–1889.
- 30. S. C. Pang, B. H. Wee and S. F. Chin, The capacitive behaviors of manganese dioxide thin-film electrochemical capacitor prototypes, Int. J. Electrochem. 2011 (2011).
- 31. Kumar, S.A., Rosaline, D.R., Foletto, E.L. et al. Application of green-synthesized cadmium oxide nanofibers and cadmium oxide/graphene nanosheet nanocomposites as alternative and efficient photocatalysts for methylene blue removal from aqueous matrix. Environ Sci Pollut Res 30, 117390–117403 (2023). https://doi.org/10.1007/s11356-023-30425-8
- 32. V. V. Deshmukh, P. A. Nagpure and D. K. Burghate, Nanoparticles, International J. Current Research, 8 (8) (2016) 35988–35991.
- 33. M. Shah, N. Khan, Z. Imran, M. Khan, A. Khattak, A. Khan and N. Ullah, Structural, optical and impedance spectroscopy study of thin film of polyaniline (PANI/ZnO) nanocomposite, Mater. Res. Express 7 (2019).
- 34. A. K. Behera, N. K. Mohanty, S. K. Satpathy, B. Behera and P. Nayak, Investigation of complex impedance and modulus properties of Nd doped 0:5BiFeO3-0:5PbTiO3 multiferroic composites, Cent. Eur. J. Phys., 12 (2014) 851-861.
- 35. M. Kashif, M. E. Ali, S. M. U. Ali, U. Hashim and S. B. Abd Hamid, Impact of hydrogen concentrations on the impedance spectroscopic behavior of Pd-sensitized ZnO nanorods, Nanoscale Res. Lett. 8 (2013) 1–9,
- 36. S. K. Barik, R. N. P. Choudhary, P. K. Mahapatra, Impedance spectroscopy study of Na1/2Sm1/2TiO 3 ceramic, Appl. Phys. Mater. Sci. Process, 88 (2007) 217–222,